Topological Graphene and the Haldane Model: A Review

Dusan Begus*
*Department of Physics, Brown University, Providence, Rhode Island, USA
(Dated: May 2024)

In this article we give an overview of several models of graphene with a focus on the underlying topology of the structures presented. After a brief overview of the tight-binding model for graphene, we go on to discuss Dirac cones and techniques used for lifting the spectral gap of the system. We analyze the symmetries of speculated models. The article builds up tools utilized in the discussion of the Haldane model which famously exhibits quantized Hall conductance without an external magnetic field. We present results of experiments probing the Haldane model in ultracold systems.

I. BACKGROUND

In 1988, F.D.M. Haldane introduced a remarkable toy model of spinless fermions on a honeycomb lattice in his classic paper "Model for a Quantum Hall Effect without Landau Levels: Condensed-Matter Realization of the Parity Anomaly ". [1]. The model is a mathematical demonstration of the integer quantum Hall effect [6]. The model in [1] has several interesting features, the most prominent one being the highly topological nature of its energy eigenstates. While most realizations of the integer quantum Hall effect require the exertion of a magnetic field and the theoretical application of Landau levels, as Haldane points out in the title of [1], such a method is not needed for the demonstration of quantized Hall conductance in his model [5]. Finally, Haldane's model is also a useful proxy for employing the Berry curvature protocol [3,4] in condensed matter physics. All of the aforementioned aspects of the model in [1] make it a fascinating theoretical phenomenon. What about the experimental realizations of the Haldane model ? While the difficulty of experimental demonstration of the Haldane model has been a major source of its criticism since the time of its publishing [2,7], a group of physicists at the Institute for Quantum Electronics at ETH Zurich published a phenomenal paper in 2014 [2], in which they showed results of an experiment done with ultracold fermions which demonstrated the effects occuring in the Haldane model.

II. ORGANIZATION OF THE PAPER

The tentative organization of the final project paper is as follows:

1. In IV we introduce the tight-binding model of graphene [8].
2. We discuss the occurrence of Dirac cones [17].
3. In V we analyze the symmetries of the tight-binding model on a hexagonal lattice [1,24].
4. In VI we demonstrate the introduction of the band gap in the tight-binding model [8] of graphene [21,24].
5. In VII we introduce the Haldane model [1]: its parity anomaly [28], sublattice symmetry breaking [1,17,21,24], and phase diagram are discussed in detail.
6. In VIII we go on to examine the sphere of experiments done with ultracold matter [30,33] in hopes of speculating their implementation in the demonstration of the Haldane model.
7. In IX we display and analyze experimental data in [2]. We will pay special attention to elliptical modulation protocols [9] and the differential drift [2] induced by Bloch oscillations [10].
8. We finish the paper by reiterating the importance of the Haldane model Hamiltonian and its impact on modern physics research.

III. ABOUT GRAPHENE

Graphene is a two-dimensional crystal with a hexagonal (honeycomb) lattice structure [14]. It consists of two overlapping triangular lattices (green and red atoms in Fig.1) with lattice vectors $\vec{b}_i$ [8]. Of great concern to us will be the three vectors $\vec{a}_i$ which indicate "hopping" from sites of one sublattice to sites on the other sublattice [8,14]. Graphene has many fascinating properties [8,14], but in this review we will only focus on a specific model with hopping parameters between first and second neighbouring atoms [1].

IV. TIGHT-BINDING FOR GRAPHENE

We now examine a tight-binding model for graphene, which will for now only include hopping between neighbouring sites of two sublattices [6,13,14,15]. The Hamiltonian reads [16,17]:

$$H = -t_1 \sum_{\vec{r}\in\Lambda} (|\vec{r}\,;A\rangle \langle \vec{r}+\vec{a}_1\,;B| + |\vec{r}\,;A\rangle \langle \vec{r}+\vec{a}_2\,;B| + \\ + |\vec{r}\,;A\rangle \langle \vec{r}+\vec{a}_3\,;B| + h.c.\,) \tag{1}$$

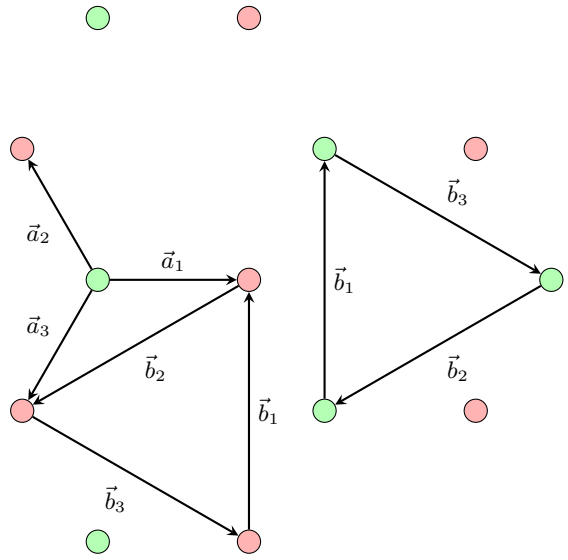

FIG. 1: Lattice structure of graphene

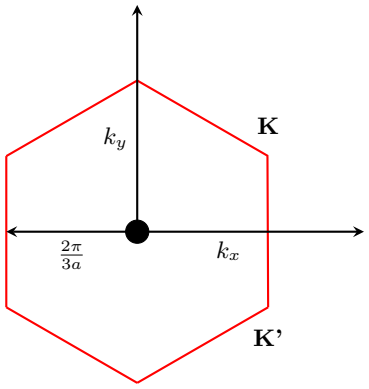

FIG. 2: The first Brillouin zone of graphene [8]. Of particular interest are points **K,K'**, which represent distinct Brillouin zone edges (they cannot be connected by a reciprocal lattice vector). We denote $|\vec{a_i}| = a$ for nearest neighbours.

where t_1 is the hopping parameter [8], and we use the notation $\left|\vec{R}\,;A\right\rangle$, $\left|\vec{R}\,;B\right\rangle$ to indicate that the state with vector $\vec{R}$ corresponds to the sublattice A or B. As usual, *h.c.* is the standard notation for a Hermitian conjugate [17]. In general, we know that the eigenstates of the Hamiltonian (1) will be Bloch wavefunctions, given by

$$\psi_{\mathbf{k}}(\mathbf{x}) = e^{i\mathbf{kx}} u_{\mathbf{k}}(\mathbf{x}) \tag{2}$$

where $u_{\mathbf{k}}(\mathbf{x})$ is a periodic function on the lattice, wih a parameter $\vec{k}$ defined in the first Brillouin zone of the reciprocal lattice [8,16,17]. Assuming a wavefunction of the form (2), one can simplify the Hamiltonian in (1) by doing computations in the first Brillouin zone of graphene (Fig.2) while working with a Hilbert space with 1/2 "spinor" [1] wavefunctions on each lattice site [17]. In particular, we will write the wavefunction Ψ as

$$\Psi(\vec{k}) = \begin{pmatrix} \Psi_A(\mathbf{k}) \\ \Psi_B(\mathbf{k}) \end{pmatrix} \tag{3}$$

where Ψ_A is the wavefunction of electrons of the reciprocal lattice of sublattice A, and Ψ_B is the wavefunction of electrons of the reciprocal lattice of sublattice B. Because of Bloch wavefunction periodicity, the wavefunction will assume the same values everywhere on the sublattices A and B; hence we supress the $\vec{x}$ indices in (3). Under the ansatz (1-3), we have the simplified Hamiltonian [1,17]:

$$H_0(\mathbf{k}) = \begin{pmatrix} 0 & \gamma(\mathbf{k}) \\ \gamma^\dagger(\mathbf{k}) & 0 \end{pmatrix} \tag{4}$$

with

$$\gamma(\mathbf{k}) = t_1 \sum_j \exp(i\mathbf{k}\cdot\mathbf{a}_j) \tag{5}$$

with index $j \in \{1,2,3\}$, acting on the wavefunction in (3). Another common form of the Hamiltonian above is in terms of Pauli matrices [1]:

$$H_0(\mathbf{k}) = t_1 \sum_i (\sigma_x \cos \mathbf{ka}_i - \sigma_y \sin \mathbf{ka}_i) \tag{6}$$

Hamiltonian (4) is easily diagonalized, and its (energy) eigenvalues are

$$E(\mathbf{k}) = \pm|\gamma(\mathbf{k})| \tag{7}$$

Taking the modulus of $\gamma(\mathbf{k})$, expression in (7) reads

$$E(\mathbf{k}) = \pm t\sqrt{1 + 4\cos\left(\frac{3k_x a}{2}\right)\cos\left(\frac{\sqrt{3}k_y a}{2}\right) + 4\cos^2\left(\frac{\sqrt{3}k_y a}{2}\right)} \tag{8}$$

Let us examine the energy bands of the tight-binding mode (Fig.3).

We can see that the two bands have zero gap at distinct momenta **K,K'** in the Brillouin zone, along with their translations by reciprocal lattice vectors. What is particularly interesting about Fig.3 is the fact that close to points **K,K'** we have relativistic excitations of the half-filled Fermi sea [8,16,17], a.k.a Dirac cones [17].

A. Physics Near the Dirac Points

In the future, it will be useful to understand what happens to the electronic excitations near points $\mathbf{K}, \mathbf{K}'$ in Fig.2 (the Dirac points).
A careful expansion of the Hamiltonian (4) around the

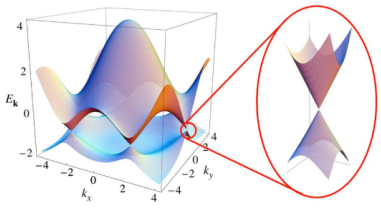

Taken from [17]

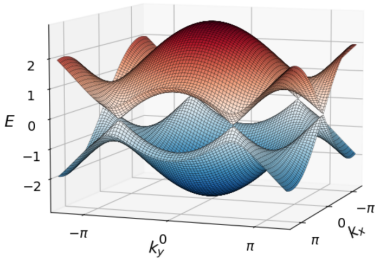

Taken from [24]

FIG. 3: Bands of the tight-binding graphene model: Two distinct Dirac cones arise at Brillouin zone edge

point **K** yields [17]:

$$H(\mathbf{q}) = v_F\hbar \begin{pmatrix} 0 & iq_x - q_y \\ -iq_x - q_y & 0 \end{pmatrix} = -v_F\hbar(q_x\sigma_y + q_y\sigma_x) \tag{9}$$

where $\mathbf{q} = \mathbf{k} - \mathbf{K}$, $v_F = \frac{3ta}{2\hbar}$, and the expansion also works out the same way around K'.
In particular, we see that excitations of graphene around the indicated Brillouin zone edges dictates the introduction of two-component relativistic spinors.

V. TOWARDS TOPOPOGICAL GRAPHENE

In this section, we want to move towards our end goal: constructing a model of graphene which exhibits integer Hall conductance **without an external magnetic field**. Since the experimental discovery of van Klitzing, Dorda and Pepper in 1982 [5], various theoretical approaches to the theory of quantized Hall conductance have been examined. All of these approaches yielded several conclusions [1,6,17,18]:

1. A material exhbiting integer Hall conductance has *topological order* [8,18]. While we will not go into the mathematical definition of topological order in this review (see [18] for a thorough review), what should be noted is that we expect non-trivial topological properties of the Brillouin zone of the model we are about to construct.

2. Integer quantum Hall samples have edge modes [5,6,8]; in particular, these excitations are chiral: they are unidirectional along the boundary of the sample. Because the integer quantum Hall sample has chiral boundary modes which break time reversal symmetry, a model exhbiting integer off-diagonal conductance also needs to break time-reversal symmetry.

Statement **2** is the most important takeaway from the conclusions listed. It tells us something important: in order to construct a model with quantized Hall conductance, we need to somehow break the time-reversal symmetry of the Hamiltonian (4). Conclusion **1** then tells us that we should look for a theory exhibiting topological order [18,19].

A. The Chiral Symmetry of the Graphene Model

Graphene is a classic example of a system with sublattice inversion symmetry (chiral symmetry) [20]. The sublattice inversion symmetry essentially "swaps" the A and B sublattices by taking the mirror image of the lattice across a line of symmetry (see figure below).

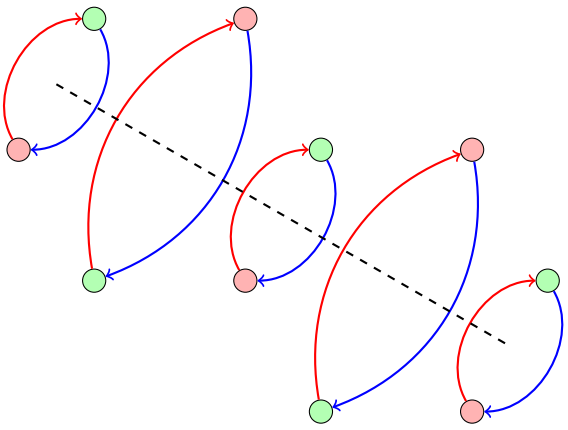

FIG. 4: The Chiral Symmetry of Tight-Binding Graphene

In terms of mathematics, the symmetry can be expressed in terms of the σ_z Pauli matrix [18]:

$$\sigma_z H(\mathbf{k})\sigma_z = -H(\mathbf{k}) \tag{10}$$

A consequence of (9) is the fact that the energy spectrum of (4) is symmetric with respect to the zero energy axis (see [17] for more detail).
In particular, if we want to construct a theory exhibiting unidirectional edge excitations like in **conclusion 2**, we need to break the sublattice symmetry of the Hamiltonian (4).

B. Time-Reversal Symmetry of the Graphene Model

Tight-binding graphene also has another symmetry: Under time reversal [24]

$$H(\mathbf{k}) \to H^{\dagger}(-\mathbf{k}) = H(\mathbf{k}) \tag{11}$$

Hence, the Hamiltonian (4) is **invariant** under time reversal.
Combining (9) and (10), we also get an additional symmetry of the Hamiltonian:

$$\sigma_z H^{\dagger}(\mathbf{k})\sigma_z = -H(\mathbf{k}) \tag{12}$$

which corresponds to the **particle-hole** symmetry near the Dirac cones. Hence, if we want to construct a model with chiral modes, we need to break the time reversal symmetry of $H(\mathbf{k})$ as well.

VI. BREAKING THE SUBLATTICE SYMMETRY: INTRODUCING A GAP

Just like was discussed in VA, in order to exhibit the integer quantum Hall effect on a hexagonal lattice, we need to somehow break the sublattice symmetry of the tight-binding model (4). We do so by creating a gap between energy bands in the system [8]. One way to fabricate the gap in (1) is by giving electrons on sites A additional energy $+M$, and decreasing the energy of electrons on sublattice B by M. This procedure is equivalent to working with the Hamiltonian [24]

$$H(\mathbf{k}) = H_0(\mathbf{k}) + \sigma_z M = \begin{pmatrix} M & \gamma(\mathbf{k}) \\ \gamma^{\dagger}(\mathbf{k}) & -M \end{pmatrix} \tag{13}$$

with σ_z the z-Pauli matrix, and

$$\gamma(\mathbf{k}) = t_1 \sum_j \exp(i\mathbf{k}\cdot\mathbf{a}_j)$$

Again, it is straightforward to diagonalize the matrix (13): the energy eigenvalues are given by

$$E(\mathbf{k}) = \pm\sqrt{t^2 + 4t^2\cos\left(\frac{3k_x a}{2}\right)\cos\left(\frac{\sqrt{3}k_y a}{2}\right) + 4t^2\cos^2\left(\frac{\sqrt{3}k_y a}{2}\right) + M^2} \tag{14}$$

We can plot (14) (see Fig.5).

The spectrum of the system is gapped; we were able to get rid of the Dirac cones. However, there is an issue: the $\sigma_z M$ term does not break time-reversal invariance. Hamiltonian (13) remains invariant under time reversal, hence it cannot contain information about chiral modes in a quantum Hall sample.

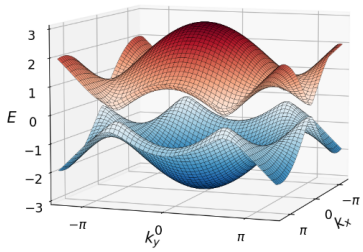

FIG. 5: Taken from [24]: Energy bands of model (13)

A. Back to the Dirac Points

What happens when we expand (13) around the Dirac points? It is trivial to incorporate the diagonal terms into the expansion of (13) around the point **K**:

$$H(\mathbf{q}) = v_F\hbar\begin{pmatrix} M & iq_x - q_y \\ -iq_x - q_y & -M \end{pmatrix} \tag{15}$$

where $\mathbf{q} = \mathbf{k} - \mathbf{K}$, $\quad v_F = \frac{3ta}{2\hbar}$.
The energies of (15) are given by

$$E_{\pm}(\mathbf{k}) = \pm v_F\hbar\sqrt{q^2 + M^2} \tag{16}$$

The eigenstates of (15) are given by [21,22,26]:

$$\psi_{\pm} = \frac{1}{\left(2(|\mathbf{q}|^2 + M^2) - 2\sqrt{|\mathbf{q}|^2 + M^2}M\right)^{(1/2)}}\begin{pmatrix} M \pm |\mathbf{q}| \\ iq_x - q_y \end{pmatrix} \tag{17}$$

Likewise, the Hamiltonian around $\mathbf{K}'$ is given by

$$H(\mathbf{q}) = v_F\hbar\begin{pmatrix} M & iq_x + q_y \\ -iq_x + q_y & -M \end{pmatrix} \tag{18}$$

$$\psi_{\pm} = \frac{1}{\left(2(|\mathbf{q}|^2 + M^2) - 2\sqrt{|\mathbf{q}|^2 + M^2}M\right)^{(1/2)}}\begin{pmatrix} M \pm |\mathbf{q}| \\ iq_x + q_y \end{pmatrix} \tag{19}$$

B. The Berry Curvature

One can mathematically track the curvature of the dispersion (16) as a function of momenta q_x, q_y: We first introduce connection vectors for the lower and upper band around **K** respectively [3,26]:

$$A_i^- = -i\left\langle\psi_-(\mathbf{k})\right|\frac{\partial}{\partial k_i}\left|\psi_-(\mathbf{k})\right\rangle \tag{20}$$

$$A_i^+ = -i\left\langle\psi_+(\mathbf{k})\right|\frac{\partial}{\partial k_i}\left|\psi_+(\mathbf{k})\right\rangle \tag{21}$$

What is incredibly fascinating about (20-21) is that $A_i^{\pm}$ takes the mathematical form of a *connection* [23] of a U(1) gauge theory. This insight was first discovered by M. Berry in his classic paper [3]. The mathematics of U(1)-bundles then tells us we can find the curvature [3,4,26] of the upper and lower bands near the Dirac point **K**:

$$\mathcal{F}_{xy}^{\pm} = \partial_x A_y^{\pm} - \partial_y A_x^{\pm} = \mathcal{F}^{\pm} = \mp \frac{M}{2(q^2+m^2)^{3/2}} \tag{22}$$

If we repeat (20-22) with the expansion around $\mathbf{K}'$ we get the following curvatures of the upper and lower band [26]:

$$\mathcal{F}'^{\pm}_{xy} = \partial_x A'^{\pm}_y - \partial_y A'^{\pm}_x = \mathcal{F}'^{\pm} = \pm \frac{M}{2(q^2+m^2)^{3/2}} \tag{23}$$

We see that the curvatures around $\mathbf{K}, \mathbf{K}'$ have **opposite signs** in the model (13), a fact which will be of great importance in the next section.

C. The Chern Number

In 1946, Chern proved a remarkable result about the integral of $\mathcal{F}$ over the the first Brillouin zone [24]:

$$\frac{1}{2\pi} \int_{\text{1st Brillouin}} d^2q \, \mathcal{F}(q) = C \in \mathbf{Z} \tag{24}$$

for any curvature $\mathcal{F}$ over a two dimensional manifold equipped with the structure of a U(1)-bundle [23].
One can think of the curvature in (21) as the curvature of the surface $E(\mathbf{k})$ (Fig.5) parameterized by k_x, k_y [8]. Using this interpretation, one can estimate that the only non-negligible contributions to the integral (21) of the curvature of Fig.5 come from the Dirac points **K,K'**. Indeed, the idea of topological robustness of a Chern insulator [1,6,8,16,21,22,26] tells us that, even if we compute an approximation of (24) for any model with a full Fermi sea [6,8], due to continuity of the curvature of a U(1) bundle [23], we should still have the integral of (22-23) over the first Brillouin zone evaluate to an integer.
We compute

$$\cdot \frac{1}{2\pi} \int d^2q \, \mp \frac{M}{2(q^2+m^2)^{3/2}} = \mp \frac{1}{2} \text{sign}(M) \tag{25}$$

where we have opposite curvatures near the two Dirac points $\mathbf{K}, \mathbf{K}'$ respectively.

D. Chern Number to Hall conductance: TKNN

In 1982, another genius result was proven: the authors were able to relate the Chen number (21) of the curvature over the first Brillouin zone to the off-diagonal conductance of the sample material [25].

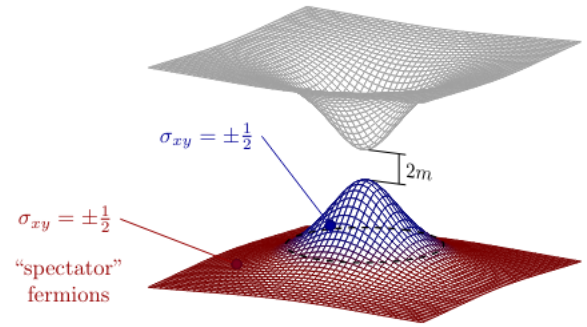

FIG. 6: Extracted from [26]: Quantum Curvature of Graphene Bands Around **K**

$$\boxed{\sigma_{xy} = -\frac{e^2}{2\pi\hbar} \sum_{\text{filled bands } \alpha} C_\alpha} \tag{26}$$

The main takeaway from (22-26) is that, for our tight-binding model of graphene with the broken sublattice symmetry (added mass terms), at half-filling (exactly one band is occupied, while the other one is empty)

$$\sigma_{xy} = \frac{1}{2}\frac{e^2}{2\pi\hbar}\text{sign}(M) - \frac{1}{2}\frac{e^2}{2\pi\hbar}\text{sign}(M) = 0 \tag{27}$$

Hence the Hall conductance of half-filled model of graphene with Hamiltonian (13) has **zero** off-diagonal conductance.

E. Failure to realize integer Hall conductance

Equation (26) tells us the model (13) fails to capture interesting topological phenomena which might occur in graphene (conclusions **1** and **2** in **V**.
A natural question is: what went wrong? Let us examine the Hamiltonian (13) more closely: it is trivial to confirm it breaks sublattice symmetry, since

$$\sigma_z \begin{pmatrix} M & \gamma(\mathbf{k}) \\ \gamma^\dagger(\mathbf{k}) & -M \end{pmatrix} \sigma_z \neq - \begin{pmatrix} M & \gamma(\mathbf{k}) \\ \gamma^\dagger(\mathbf{k}) & -M \end{pmatrix}$$

What about time reversal invariance? We have

$$\begin{pmatrix} M & \gamma(-\mathbf{k}) \\ \gamma^\dagger(-\mathbf{k}) & -M \end{pmatrix}^\dagger = \begin{pmatrix} M & \gamma(\mathbf{k}) \\ \gamma^\dagger(\mathbf{k}) & -M \end{pmatrix} \tag{28}$$

So Hamiltonian (13) is **time-reversal invariant**.
Hence, according to Sec.V, it **cannot** contain information about the chiral edge modes of the integer quantum Hal sample [24].

F. Band Engineering

We might ask ourselves: how does one engineer the band in Fig.5 so that the Berry curvature around point

K switches sign? If one can manipulate the Berry curvature of (14), then the Chern number the graphene model should become nontrivial, hence admitting integer Hall conductance plateaux. We essentially need different values of gaps at $\mathbf{K}, \mathbf{K}'$ so that gap closings in the spectrum become independent under variations of model parameters. In the next chapter, we explore a specific model exhbiting sublattice and time reversal symmetry breaking, along with a highly malleable energy band.

VII. THE HALDANE MODEL

F.D.M. Haldane's ingenuity came into the spotlight in 1988 when he added **another term** to the Hamiltonian (13): he considered second-nearest neighbour hoppings to (13,14) in the following way [1]:

$$\boxed{H(\vec{k}) = H_0(\vec{k}) + M\sigma_z + 2t_2 \sin\phi \sum_i \sigma_z \sin\left(\vec{k}\cdot\vec{b}_i\right)} \tag{29}$$

where $\phi \in [0, 2\pi)$ is an angular parameter which enables us to track different phases of the system [1].
What (29) represents physically is a tight-binding model with added second-nearest neighbour interaction (see Fig. 7) [21].

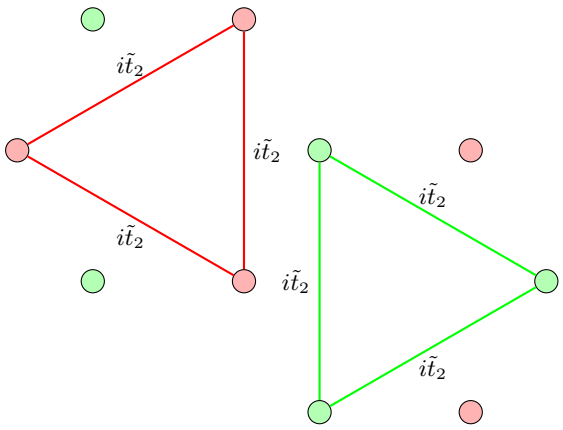

FIG. 7: Second-nearest neighbour interactions in the Haldane model: $\tilde{t}_2 = t_2 \sin\phi$

We can write the Hamiltonian of the Haldane model in k-space as [1]:

$$H(\mathbf{k}) = \begin{pmatrix} M + \tilde{t}_2 \sum_i \sin\left(\mathbf{k}\mathbf{b}_i\right) & t_1 \sum_i \exp(i\mathbf{k}\mathbf{a}_i) \\ t_1 \sum_i \exp(-i\mathbf{k}\mathbf{a}_i) & -M - \tilde{t}_2 \sum_i \sin\left(\mathbf{k}\mathbf{b}_i\right) \end{pmatrix} \tag{30}$$

with the hopping parameter

$$\tilde{t}_2 = t_2 \sin\phi \tag{31}$$

Hamiltonian (29) is easily verified to **break both sublattice and time-reversal symmetries of graphene** [1,17,22].
It is straightforward to diagonalize (29)

$$E(\mathbf{k}) = \pm\sqrt{t_1^2 + 4t_1^2 \cos\left(\frac{3k_x a}{2}\right)\cos\left(\frac{\sqrt{3}k_y a}{2}\right) + t_1^2 4\cos^2\left(\frac{\sqrt{3}k_y a}{2}\right) + \tilde{M}^2} \tag{32}$$

with

$$\tilde{M}(\mathbf{k}) = M + t_2 \sin\phi \sum_i \sin\left(\mathbf{k}\mathbf{b}_i\right) \tag{33}$$

We immediately see that the only points at which the gap in (32) may close are $\mathbf{K}, \mathbf{K}'$ of the first Brillouin zone. There are exactly two values of t_2 for which we get gap closings in the spectrum of (32-33):

1. Gap closing at $\mathbf{K}'$ for $\tilde{t}_2 = -M/3\sqrt{3}$
2. Gap closing at $\mathbf{K}$ for $\tilde{t}_2 = M/3\sqrt{3}$

A. Berry Curvature and the Chern Number of the Haldane Model

Near the point $\mathbf{K}'$, in the limit $M \to \infty$, we can approximate the Hamiltonian (29) by [26]

$$H(\mathbf{q}) = -\frac{3}{2}t_1 a(q_y\sigma_x + q_x\sigma_y) + (M + 3\sqrt{3}t_2 \sin\phi)\sigma_z \tag{34}$$

with $\mathbf{q} = \mathbf{k} - \mathbf{K}'$.
Likewise, expanding around $\mathbf{K}$ in the large M limit:

$$H(\mathbf{q}) = \frac{3}{2}t_1 a(q_y\sigma_x - q_x\sigma_y) + (M - 3\sqrt{3}t_2 \sin\phi)\sigma_z \tag{35}$$

Repeating the same procedure as in (VI.B- VI.D), one can then make the assumption that the Berry curvature only gives a nonvanishing contribution to the Chern number of the **half-filled band** in (32) around the two Dirac points $\mathbf{K}, \mathbf{K}'$, thus arriving at the following result equivalent to the computation (20-26):

$$C_{\text{Haldane}} = \frac{1}{2\pi}\int d^2q\, \mathcal{F}(q) + \frac{1}{2\pi}\int d^2q\, \mathcal{F}'(q) =$$

$$= -\frac{1}{2}\text{sign}(M - 3\sqrt{3}\tilde{t}_2) + \frac{1}{2}\text{sign}(M + 3\sqrt{3}\tilde{t}_2) \tag{36}$$

B. Phase Diagram of the Haldane Model

One can use equation (36) and the TKNN formula (26) to write the Hall conductance of the sample as

$$\sigma_{xy} = +\frac{e^2}{2\pi\hbar}\left(\frac{1}{2}\text{sign}(M - 3\sqrt{3}\tilde{t}_2) - \frac{1}{2}\text{sign}(M + 3\sqrt{3}\tilde{t}_2)\right) \tag{37}$$

One can then plot σ_{xy} as a function M/t_2 and ϕ (Fig.8): We see that the system experiences three different phases as M/t_2 and ϕ are varied.
What we essentially observe is the **integer quantum Hall effect** [5,6] without an *external magnetic field* applied to the system [1]. To quote F.D.M. Haldane in [1]: *while the particular model presented here is unlikely to be directly physically realizable, it indicates that, at least in principle, the QHE can be placed in the wider context of phenomena associated with broken timereversal invariance, and does not necessarily require external magnetic fields, but could occur as a consequence of magnetic ordering in a quasi-two-dimensional system.*

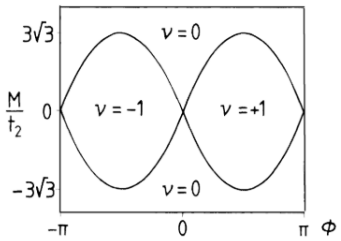

FIG. 8: Extracted from [1]: The Phase Diagram of the Haldane Model

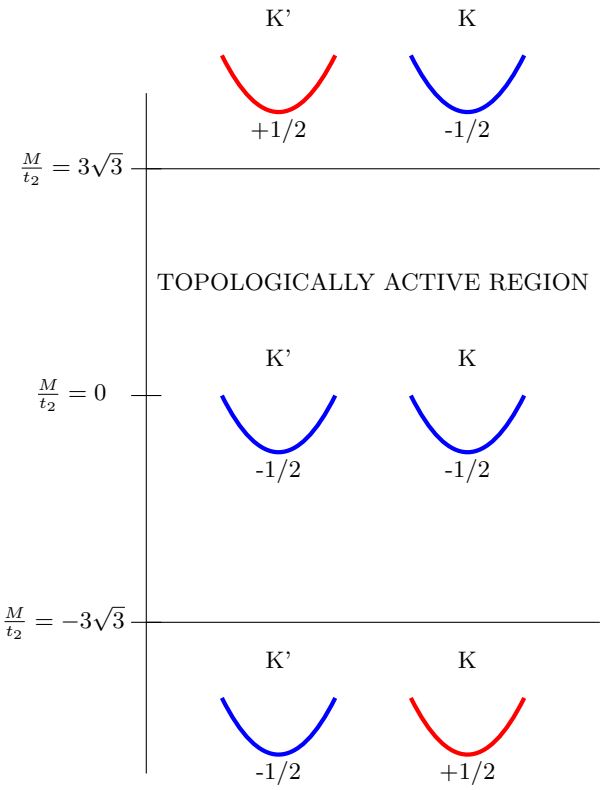

FIG. 9: The phase diagram of the Haldane model for $\phi = -\pi/2$: Chern numbers around the Dirac points are shown

VIII. ULTRACOLD PARTICLES IN THE REAL WORLD

A natural realization of numerous quantum many-body systems arises through the implementation of ultracold particles [29]. Several theoretical models of quantum phase transitions of fermions in two dimensions (including the Haldane model topological phase transition [1,2]) work at zero temperature, at which fermions are clustered into states below the Fermi energy [8], whilst also maintaining neighbouring site interactions [1]. Preparing ultracold particle systems enables for optimal simulation and control of such systems [29]. Therefore, it is not strange that in 2014, a group of scientists at ETH Zurich constructed a successful realization of the Haldane model using laser-cooled systems [2]. Before we delve into the specifics of the techniques in [2] and subsequent measurements performed, we first need to address hard work which goes into transforming real matter structures into ultracold systems:

1. The first obstacle to creating ultracold systems is rather obvious: One needs to cool atomic systems to ultracold temperatures (from $T \sim 10^{-9}K$ (Cornell, Ketterle, Wieman [30,33] to higher temperatures $T \sim 10^{-6}K$ (Chu,Philips, Tannoudji [31]).
One performs the process of cooling by holding fermionic/bosonic quasiparticles (for example ^6Li or ^{40}K atoms [32,33]) in a trapping potential whose potential enery barrier can be controlled [29]. Atoms with high energies then leave the trap through the process of quantum tunneling [8], leaving only low-energy particles in the system.
The whole procedure is meticulously hard to achieve, which is why it is currently only being performed at specialized scientific facilities across the world. However, W. Ketterle remains a proponent of the idea of technologically manufacturing materials which work at ultracold temperatures to build various exciting quantum devices [33].

2. In order for the ultracold fermions to simulate systems at zero temperature, one needs to assume that the theory of interest agrees with the Landau theory of Fermi liquid [8] at cold temperatures: the spectral flow of the eigenstates of the system Hamiltonian should not experience any level crossings in the interval between the ultracold temperature (see above) and zero temperature. This rather small (but important) remark has been a subject of many investigations probing the validity of results of ultracold experiments [29,30,31,32,33].

3. In order to realistically isolate models with weak interactions, one needs to decrease the s-wave scattering length a of the particles [33]. This is implemented through the use of fermionic spin mixtures

with Feshbach resonance [34] whilst also controlling the particle positions by invoking electric field Bloch oscillations [8,10].

IX. EXPERIMENTAL REALIZATION OF THE HALDANE MODEL

We finally review an experimental demonstration of the Haldane model [2]. We will make an effort to give an honest review of the group's work while also relying on numerics.

A. Materials and Setup

The group at ETH Zurich worked with a noninteracting, ultracold gas of 4×10^4 fermionic ^{40}K atoms prepared in the lowest band of a honeycomb *optical* lattice created by several laser beams at wavelength $\lambda = 1064nm$, arranged in the XY plane as depicted in Fig.10 [2]: Just

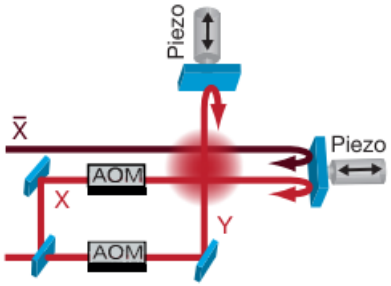

FIG. 10: Extracted from [2]: Quoting [2]: *Piezoelectric actuators sinusoidally modulate the retro-reflecting mirrors, with a controllable phase difference ϕ. Acousto-optic modulators (AOMs) ensure the stability of the lattice geometry*

like in the theoretical prediction, we will get the two lowest bands separate themselves energetically from the rest of the spectrum, with their total bandwidth $h\cdot 3.9kHz$ and a gap of $h\cdot 5.4kHz$ to the next higher band. Between the two energetic bands lie the Dirac points, just like in Fig.2.
In particular, the trapping potential used to confine the atoms into a honeycomb structure had the following form

$$V(x,y,z) = -V_{\bar{X}}\cos^2 k_L x + \theta/2 - V_X\cos^2 k_L x -$$

$$-V_Y\cos^2 k_L y - V_{\bar{Z}}\cos^2 k_L z -$$

$$-2\alpha\sqrt{V_X V_Y}\cos k_L x\cos k_L y\cos\phi_L \qquad (38)$$

where $V_{X,\bar{X},Y,\bar{Z}}$ are single-beam lattice depths and $k_L = 2\pi/\lambda$ [2]. The timescale for this process is roughly $t\sim$ 300ms.

B. Elliptical Modulation

Let us now delve into the specifics of the elliptical modulation protocol [9] performed in [2].
The group mounted a mirror on each of the piezo-electric actuators to retro-reflect the lattice beams. The piezo-electric components allow for a controlled phase shift of the reflected beams with respect to incident beams [2]. The relative phase between the incoming and the outgoing beam was set to be $\phi_L = 0$ during the entire course of the experiment.
The modulation is then activated in the following steps: The atoms are inserted into the lattice with 30% stronger confining potential than the one used in the experiment. We immediately thus stop atoms from transitioning into higher bands. The modulation of the amplitude is increased every $20ms$ to reach the drive $K_0 = 0.7778$, where we have $K_0 = \pi^2 A\hbar\omega/\lambda E_R$, with ω the modulation angular frequency and $E_R = h^2/2m\lambda^2$, with m the mass of ^{40}K.
The lattice positions are then given by the formula [2]:

$$\mathbf{r}_{\text{lat}} = -A(\cos\omega t\mathbf{e}_x + \cos(\omega t - \phi_L)\mathbf{e}_y) \qquad (39)$$

C. Floquet Theory Model Modulation: The Big Idea

After placing the atoms in a honeycomb lattice, we turn on a sinusoidal modulation of the lattice position along the x and y axes with amplitude 0.087λ, frequency $4.0kHz$ and **phase difference** $\phi\in\{0,-\pi/2,\pi/2,\pi\}$.
Using Floquet theory [35], one can compute the effective Hamiltonian of the phase-modulated honeycomb lattice to be [2]:

$$\hat{H} = \sum_{\langle ij\rangle} t_{ij}\hat{c}_i^\dagger\hat{c}_j + \sum_{\langle\langle ij\rangle\rangle} e^{i\Phi_{ij}}t'_{ij}\hat{c}_i^\dagger\hat{c}_j + \Delta_{AB}\sum_{i\in A}\hat{c}_i^\dagger\hat{c}_i \qquad (40)$$

where t_{ij} and t'_{ij} are real valued nearest-neighbour and next nearest-neighbour hopping parameters respectfully. One can immediately see the role of the parameters Φ_{ij}: if tuned right, they will give us the same hopping parameters present in the Haldane model (29). The terms Δ_{AB} serves to create an offset between lattice sites in sublattices A and B (in the Haldane model (29), we will have $\Delta_{AB} = \pm M$ depending on whether we work with right-handed or left-handed component of the spinor in (30) respectfully.
By the theoretical analysis in section VII of the paper, we then know that we get topological phase transitions at

$$\frac{\Delta}{t'} = \pm 3\sqrt{3}\sin\Phi \qquad (41)$$

if we take uniform couplings $t'_{ij} = t', \Delta_{AB} = \Delta($ on sublattice A $), \Phi_{ij} = \Phi$.

D. How to measure the Berry Curvature

We are now faced with the natural question of measuring the Berry curvature of the Hamiltonian (40) in our ultracold system. To compute the effective Hamiltonian (40) in real time, one first lets the system evolve over one modulation period in IXa, and then takes the logarithm of the evolved wavefunction of the system, giving the correct Hamiltonian by perturbation theory [8]. Numerically, we will discretise momentum space **q** in a high resolution to observe the changes in momentum when an electric field is turned on. Again, we remember that the Haldane model **does not require** the exertion of an outside magnetic field. The semiclassical equations of motion for the atoms read [2,8]

$$\dot{x} = \frac{1}{\hbar}\partial_{q_x}\epsilon(q_x, q_y) - \dot{q}_y\Omega(q_x, q_y)$$

$$\dot{y} = \frac{1}{\hbar}\partial_{q_y}\epsilon(q_x, q_y) + \dot{q}_x\Omega(q_x, q_y)$$

$$\hbar\dot{q}_x = -\partial_x V_{\text{trap}}(x, y, z)$$

$$\hbar\dot{q}_y = F_y - \partial_y V_{\text{trap}}(x, y, z) \tag{42}$$

where V_{trap} is the trapping potential defined in (38), F_y is an external accelerating force parameter [2], and $\epsilon(q_x, q_y)$ is the spectral function of the system. Finally, $\Omega(q_x, q_y)$ is the **Berry curvature** of the band [8].
We can see that the **semiclassical equations of motion** provide a natural computational interpretation of the Berry curvature Ω. In the absence of the curvature (Ω=0), the atoms will undergo position space **Bloch oscillations** [2,8,10], i.e. they will start to oscillate when an equivalent of the external electric field is applied to the system, a.k.a. the accelerating force parameter in (42). Non-zero Berry curvature induces a **drift** in the motion of the atoms: the atoms will oscillate due to the same terms that cause Bloch oscillations, but now the centres of oscillations will follow a decoupled curve with its tangent orthogonal to $\nabla\Omega$. This allows for tracking the motion of the atoms and hence measuring Berry curvature of the bands of the Hamiltonian (40) to great precision [2].

E. Results

From the last section we infer that the differential drift $\mathcal{D}$ (the rate at which the oscillation centers of the atoms move) is **proportional** to the **Berry curvature** of the material's band. One can then measure the mean differential drift of the atoms in a random phase space configuration, arriving at the following diagram (Fig.11): Per our earlier discussion, the heat map in *Fig.*11**a)** should be "proportional" to the phase diagram of the Haldane model in Fig.8. Comparing the two figures, we observe

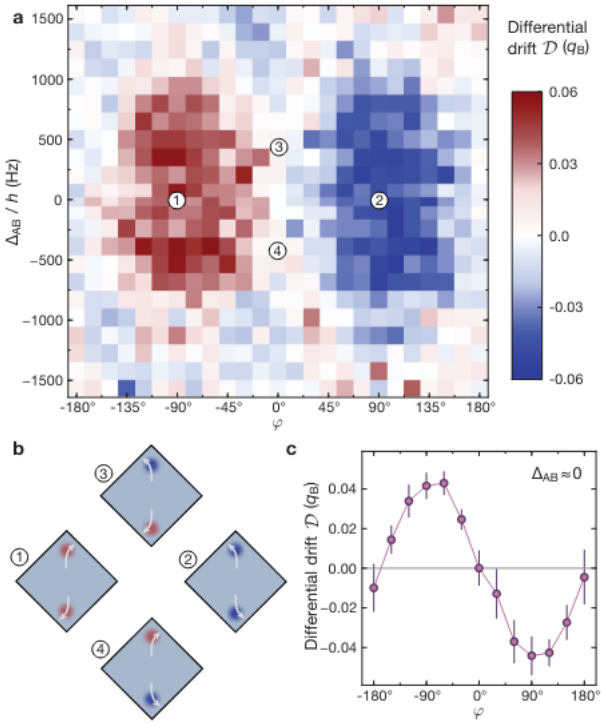

FIG. 11: Extracted from [2]:
a) Heat map of the differential drift of the sample with respect to parameters Φ, Δ_{AB}. h is the Planck constant.
b) Quoting [2]: all topological regimes are explored and the expected momentum-space drifts caused by the Berry curvature are sketched for selected parameters.
c) Quoting [2]: cut along the $\Delta_{AB}/h = 15.7$Hz line. Data show mean ± standard deviation of at least 6 pairs of measurements.

clear evidence of the same critical surfaces between the ultracold ^{40}K atom honeycomb lattice system and in the Haldane model. Hence, a successful demonstration of the Haldane model has indeed been realized.

X. DISCUSSION

In this paper, we were able to approach several theoretical and experimental techniques utilized in the treatment of topological graphene models and the Haldane model [1,2,8,14]. Since Haldane published his paper in 1988, many other models demonstrating the integer quantum Hall effect with zero external magnetic field have been discovered, but the essence of geometric ideas underlying any of those structures can be extrapolated from a toy model of the graphene lattice with second nearest-neighbour interactions. Hence, Haldane's model has stood the test of time as a remarkable discovery in modern physics.

[1] Haldane FD. *Model for a quantum Hall effect without Landau levels: Condensed-matter realization of the "parity anomaly".* Phys Rev Lett. 1988 Oct 31;61(18):2015-2018. doi: 10.1103/PhysRevLett.61.2015. PMID: 10038961.

[2] Jotzu, G., Messer, M., Desbuquois, R. et al. *Experimental realization of the topological Haldane model with ultracold fermions.* Nature 515, 237–240 (2014). https://doi.org/10.1038/nature13915

[3] Berry, M. V. *"Quantal Phase Factors Accompanying Adiabatic Changes."* Proceedings of the Royal Society of London. Series A, Mathematical and Physical Sciences 392, no. 1802 (1984): 45–57. http://www.jstor.org/stable/2397741.

[4] Michel, Simon, and Michael Potthoff. *"Spin Berry curvature of the Haldane model."* Physical Review B 106.23 (2022): 235423.

[5] K. von Klitzing, G. Dorda and M. Pepper, *New method for high accuracy determination of the fine structure constant based on quantized Hall resistance* Phys. Rev. Lett. 45, 494-497 (1980)

[6] Tong, David. *"Lectures on the quantum Hall effect."* arXiv preprint arXiv:1606.06687 (2016).

[7] Kim, Heung-Sik, and Hae-Young Kee. *"Realizing Haldane model in Fe-based honeycomb ferromagnetic insulators."* npj Quantum Materials 2.1 (2017): 20.

[8] Girvin, Steven M. and Kun Yang. *"Modern Condensed Matter Physics."* (2019).

[9] Song, C., and Shimamoto, S. (2004). *Evaluations of elliptical modulation scheme.* In 2004 IEEE Wireless Communications and Networking Conference, WCNC 2004 (pp. 1176-1181). (2004 IEEE Wireless Communications and Networking Conference, WCNC 2004; Vol. 2). Institute of Electrical and Electronics Engineers Inc.. https://doi.org/10.1109/wcnc.2004.1311355

[10] Phong, Vo Tien, and E. J. Mele. *"Quantum Geometric Oscillations in Two-Dimensional Flat-Band Solids."* Physical Review Letters 130.26 (2023): 266601. Phys. Rev. B 98, 155134 – Published 22 October 2018

[11] Lapa, Matthew F. *"A note on the parity anomaly from the Hamiltonian point of view."* arXiv preprint arXiv:1903.06719 (2019).

[12] Chern, Shiing-Shen (1946), *Characteristic classes of Hermitian Manifolds*, Annals of Mathematics, Second Series, 47 (1): 85–121

[13] M. Nakahara, *Geometry, topology and physics* (2003)

[14] Novoselov, K. S. "Nobel lecture: Graphene: Materials in the flatland." Reviews of modern physics 83.3 (2011): 837.

[15] Uppstu, Andreas. *Electronic properties of graphene from tight-binding simulations.* (2014).

[16] Sigrist, Manfred. "Solid state theory." Lecture notes, ETH Zürich 47 (2013).

[17] Tong, David. *Lectures on Solid State Physics* https://www.damtp.cam.ac.uk/user/tong/aqm/solidstate.pdf Accessed Apr 2024

[18] Hastings, Matthew B. *Locality in quantum systems.* Quantum Theory from Small to Large Scales 95 (2010): 171-212.

[19] Brandao, Fernando GSL, and Michał Horodecki. *Exponential decay of correlations implies area law.* Communications in mathematical physics 333 (2015): 761-798.

[20] Semenoff, Gordon W. "Chiral symmetry breaking in graphene." Physica Scripta 2012.T146 (2012): 014016.

[21] *Topological Quantum Matter Online Course*, Weizmann Institute https://www.weizmann.ac.il/condmat/Events/20 Accessed May 2024

[22] Haldane, F. Duncan M. "Nobel lecture: Topological quantum matter." Reviews of Modern Physics 89.4 (2017): 040502.

[23] Vákár, Matthijs. "Principal bundles and gauge theories." arXiv preprint arXiv:2110.06334 (2021).

[24] Online Course on Topology in Condensed Matter *Topology in Condensed Matter: Tying quantum knots; Haldane Model, Berry Curvature, and Chern Number* https://topocondmat.org/index.html Accessed May 2024

[25] Thouless, David J., et al. "Quantized Hall conductance in a two-dimensional periodic potential." Physical review letters 49.6 (1982): 405.

[26] S. Huber, T. Neupert *Lecture Notes: Topological Condensed Matter Physics* https://ethz.ch/content/dam/ethz/special-interest/phys/theoretical-physics/cmtm-dam/documents/tqn/tqn-2021/TopCondMat.pdf Accessed May 2024

[27] Adachi, Keisuke, and Minoru Kanega. *TopologicalNumbers. jl: A Julia package for topological number computation.* arXiv preprint arXiv:2402.00885 (2024).

[28] Witten, Edward. *The "parity" anomaly on an unorientable manifold.* Physical Review B 94.19 (2016): 195150.

[29] Bloch, Immanuel, Jean Dalibard, and Wilhelm Zwerger. *Many-body physics with ultracold gases.* Reviews of modern physics 80.3 (2008): 885.

[30] Cornell, Eric A., and Carl E. Wieman. *Nobel Lecture: Bose-Einstein condensation in a dilute gas, the first 70 years and some recent experiments.* Reviews of Modern Physics 74.3 (2002): 875.

[31] Srinivasan, R. *1997 Nobel Prize for Physics: Laser cooling and trapping of atoms.* Current Science 74.2 (1998): 106-110.

[32] Georges, Antoine, and Thierry Giamarchi. *Strongly correlated bosons and fermions in optical lattices.* arXiv preprint arXiv:1308.2684 (2013).

[33] Ketterle, Wolfgang. *Nobel lecture: When atoms behave as waves: Bose-Einstein condensation and the atom laser.* Reviews of Modern Physics 74.4 (2002): 1131.

[34] Chin, Cheng, et al. *Feshbach resonances in ultracold gases.* Reviews of Modern Physics 82.2 (2010): 1225.

[35] Barone, S. R., M. A. Narcowich, and F. J. Narcowich. *Floquet theory and applications.* Physical Review A 15.3 (1977): 1109.